

Sensitivity enhancement of micro-optical gyro with photonic crystal

Liu Yang(杨柳), Shuhua Zhao(赵舒华), Jingtong Geng(耿靖童), Bing Xue(薛冰), and Yonggang Zhang(张勇刚)
Citation: Chin. Phys. B, 2021, 30 (**4**): 044208. DOI: 10.1088/1674-1056/abe3f3
Journal homepage: http://cpb.iphy.ac.cn; http://iopscience.iop.org/cpb

What follows is a list of articles you may be interested in

Generation of wideband tunable femtosecond laser based on nonlinear propagation of power-scaled mode-locked femtosecond laser pulses in photonic crystal fiber

Zhiguo Lv(吕志国) and Hao Teng(滕浩)
Chin. Phys. B, 2021, 30 (**4**): 044209. DOI: 10.1088/1674-1056/abe231

High-precision three-dimensional atom localization via probe absorption at room temperature

Mengmeng Luo(罗萌萌), Wenxiao Liu(刘文晓), Dingyu Cai(蔡定宇), and Shaoyan Gao(高韶燕)
Chin. Phys. B, 2020, 29 (**12**): 124205. DOI: 10.1088/1674-1056/abb3df

Thermal tunable one-dimensional photonic crystals containing phase change material

Yuanlin Jia(贾渊琳), Peiwen Ren(任佩雯), and Chunzhen Fan(范春珍)†
Chin. Phys. B, 2020, 29 (**10**): 104210. DOI: 10.1088/1674-1056/abab78

A compact electro-absorption modulator based on graphene photonic crystal fiber

Guangwei Fu(付广伟), Ying Wang(王颖), Bilin Wang(王碧霖), Kaili Yang(杨凯丽), Xiaoyu Wang(王晓愚), Xinghu Fu(付兴虎), Wa Jin(金娃), Weihong Bi(毕卫红)
Chin. Phys. B, 2020, 29 (**3**): 034209. DOI: 10.1088/1674-1056/ab6838

Design of diamond-shape photonic crystal fiber polarization filter based on surface plasma resonance effect

Yongxia Zhang(张永霞), Jinhui Yuan(苑金辉), Yuwei Qu(屈玉玮), Xian Zhou(周娴), Binbin Yan(颜玢玢), Qiang Wu(吴强), Kuiru Wang(王葵如), Xinzhu Sang(桑新柱), Keping Long(隆克平), Chongxiu Yu(余重秀)
Chin. Phys. B, 2020, 29 (**3**): 034208. DOI: 10.1088/1674-1056/ab683c

---

Sensitivity enhancement of micro-optical gyro with photonic crystal*

Liu Yang(杨柳), Shuhua Zhao(赵舒华), Jingtong Geng(耿靖童), Bing Xue(薛冰)†, and Yonggang Zhang(张勇刚)

College of Intelligent Systems Science and Engineering, Harbin Engineering University, Harbin 150001, *China*

(Received 4 January 2021; revised manuscript received 23 January 2021; accepted manuscript online 8 February 2021)

We propose a core rotation-sensing element for improving the sensitivity of the micro-optical gyroscope using the large nonreciprocal effect with a photonic crystal. The sharp transmission peak of electromagnetically induced transparency in photonic crystal generated from a periodic distribution of cold atoms is sensitive to the rotation. Our numerical results show that the sensitivity of relative rotation is about 50 times higher and the sensitivity of absolute rotation is more than two orders higher than that of the traditional resonant optical gyroscope. Also, the sensitivity of the gyroscope can be manipulated by varying the atomic density, modulation frequency, probe pulse width, and photonic crystal length, etc.

Keywords: optical nonreciprocal effect, photonic crystal, micro-optical gyro, high sensitivity

PACS: 42.50.Gy, 42.70.Qs, 42.79.Gn, 42.81.Pa **DOI:** 10.1088/1674-1056/abe3f3

1. Introduction

Inertial sensors for rotation such as ring laser gyros (RLG), interferometric optical gyroscopes (IOG), and micro-electro-mechanical system (MEMS) gyros are now widely used in commercial and military fields. Miniaturized inertial measurement units enable small platforms for a variety of emerging applications, such as unmanned air and underwater vehicles, as well as navigation in subterranean structures. As MEMS-based sensors do not provide sensitivity that competes with optical gyros, a variety of micro-optical gyros, such as ring micro-laser gyros,[1] fiber ring resonator micro-optical gyros,[2] micro-resonator Brillouin gyros,[3,4] parity time (PT) symmetric microscale optical gyros,[5,6] non-Hermitian ring laser gyroscopes,[7] and waveguide micro-ring resonate gyros[8–12] have been recently demonstrated.

While many researchers make great efforts in micro-optical gyros, the ultimate goal of high sensitivity has not been previously realized.[13,14] IOG and RLG with high sensitivities are difficult to be miniaturized,[15] so resonant micro-optical gyro (RMOG) and Brillouin micro-optic gyro (BMOG) with a chip-based optical resonator were introduced as the ideal candidates for new generation optical gyros with high sensitivity, miniaturization.[1,3,16,17] However, immature detection technique[18] and low signal-to-noise ratio[19] result in the RMOG and BMOG still in the stage of laboratory research with lower sensitivities compared with the mature RLG and IOG. Therefore, it is very important and urgent to propose a new structure or detection method to improve the sensitivity of micro-optical gyros.

Electromagnetically induced transparency (EIT),[20] a quantum interference effect induced by a strong coupling field, based on which the optical absorption of a weak probe field can be largely suppressed in a small frequency range while the large-dispersion property remains. Recently, the study of EIT has been extended to atoms confined in optical cavities[21,22] and impurities doped in photonic bandgap (PBG) materials,[23,24] and singular electromagnetic modes in cavities and at band edges may be utilized to control and modify EIT features. Petrosyan's work[25] showed that very narrow bandgap and transmission peak might arise within the transparent window.

Great efforts have been made to achieve optical nonreciprocity, such as using media with P-T symmetry,[26–28] with acousto-optical effects[29] or magneto-optical effects,[3] using spinning resonators,[31–34] and using nonsymmetric photonic crystals.[35] Recently, it has been found that the nonreciprocal transmission can be achieved by setting the photonic crystal[36] and periodically distributed atoms into motion.[37,38] When a photonic crystal moves, the counter-propagating light is blueshifted and the co-propagating light is redshifted in the reference frame of the moving photonic crystal due to the Doppler effect.[38]

According to the working principle of RMOG, the resonance frequency difference related to angular velocity is determined by the Sagnac effect, while the detection sensitivity depends on the fineness of the resonator (namely, the slope of the demodulation curve).[11] The resonance frequency difference is fixed when the size of the resonator is defined, so improving the fineness of the core sensing element is a good way to improve the sensitivity of gyros.

In this paper, we extend the previous works[37,38] and improve the sensitivity of micro-optical gyros by using the

*Project supported by the National Natural Science Foundation of China (Grant Nos. 11804066 and 61773133), Heilongjiang Provincial Natural Science Foundation of China (Grant No. LH2019A005), China Postdoctoral Science Foundation (Grant No. 2018M630337), and Heilongjiang Provincial Postdoctoral Science Foundation (Grant No. LBHZ18062).

†Corresponding author. E-mail: xuebinghrbeu@163.com

© 2021 Chinese Physical Society and IOP Publishing Ltd

photonic crystal. ^{87}Rb atoms driven into a three-level Λ configuration, periodically trapped into the photonic crystal, may create a sharp transmission peak of electromagnetically induced transparency. We discuss the generation of large clockwise-counterclockwise (CW-CCW) nonreciprocal transmission, which leads to improving the sensitivity of the gyro system. In addition, it is discussed that the sensitivity depends on the slope of nonreciprocal curve could be controlled by varying the atomic density, modulation frequency, probe pulse width, and photonic crystal length, etc.

2. Theoretical models and equations

Refer to the D2 of ^{87}Rb atoms, we study a threelevel Λ atomic system where levels $|1\rangle$, $|2\rangle$, and $|3\rangle$ correspond to states $|5S_{1/2}, F=2\rangle$, $|5S_{1/2}, F=1\rangle$, and $|5S_{3/2}, F=2\rangle$, respectively, as shown in Fig. 1(a). The atomic transition between level $|3\rangle$ and level $|1\rangle$ is coherently driven by a probe (coupling) field. The probe field $\omega_{\rm p}$ is detuned from atomic transition $|3\rangle \to |1\rangle$ by $\Delta_{\rm p} = \omega_{31} - \omega_{\rm p}$, and the coupling field $\omega_{\rm c}$ is detuned from atomic transition $|3\rangle \to |2\rangle$ by $\Delta_{\rm c} = \omega_{32} - \omega_{\rm c}$.

Under the electric-dipole and rotating-wave approximations, the interaction Hamiltonian can be rewritten as

$$\begin{aligned} H(t) \;=\; & \hbar\big[\Delta_{\rm p}|1\rangle\langle 1| + \big(\Delta_{\rm p} - \Delta_{\rm c}\big)|2\rangle\langle 2| \\ & -\Omega_{\rm c}|2\rangle\langle 3| - \Omega_{\rm p}|1\rangle\langle 3| + {\rm c.c.}\big], \end{aligned} \tag{1}$$

from which it is straightforward to attain 16 dynamic equations for the mutually coupled density matrix elements ρ_{hk} with $h,k \in \{1,2,3\}$. In the weak probe limit, the above density matrix equations can be reduced into

$$\partial_t \rho_{12} = -[\gamma_{12} - {\rm i}(\Delta_{\rm p} - \Delta_{\rm c})]\rho_{12} - {\rm i}\Omega_{\rm c}\rho_{13}, \tag{2a}$$

$$\partial_t \rho_{13} = -(\gamma_{13} - {\rm i}\Delta_{\rm p}) - {\rm i}\Omega_{\rm c}^{*}\rho_{12} - {\rm i}\Omega_{\rm p}^{*}. \tag{2b}$$

Here, γ_{hk} is the decay rate of atomic coherence on transition $|h\rangle \leftrightarrow |k\rangle$. Thus, we can solve Eq. (2) analytically in the steady state ($\partial_t \rho_{hk}$) to obtain the probe susceptibility

$$\begin{aligned} \chi_{\rm p}(x) &= \frac{N(x)|d_{13}|^2}{2\varepsilon_0\hbar}\cdot\frac{\rho_{13}}{\Omega_{\rm p}} \\ &= \frac{N(x)|d_{13}|^2}{2\varepsilon_0\hbar}\cdot\frac{{\rm i}\gamma_{12} + (\Delta_{\rm p} - \Delta_{\rm c})}{[\gamma_{12} - {\rm i}(\Delta_{\rm p} - \Delta_{\rm c})](\gamma_{13} - {\rm i}\Delta_{\rm p}) + \Omega_{\rm c}^2}, \end{aligned} \tag{3}$$

where $N(x)$ is the inhomogeneous atomic density as a periodic function of the photonic crystal length x.

Photonic crystal is generated from a periodic distribution of ^{87}Rb atoms as shown in Fig. 1(b), while each period of the photonic crystal exhibits a small Gaussian density distribution $N_a(x) \propto 1/\sqrt{2\pi\sigma_x}N_0 \exp[-(x-a/2)^2/2\sigma_x^2]$ with rms width $\sigma_x = \lambda_{31}/(2\pi\sqrt{2\eta})$ along the photonic crystal length x in $-a/2 \le x \le a/2$, and $a = d/n$ being the length of each period. Figure 1(c) shows a core sensing element of gyro for relative rotation sensing. Due to the Doppler effect, the photonic crystal may lead to a strong nonreciprocity[37,38] to enhance the sensitivity of relative rotation between the propagation medium and the rest of the gyro. Figure 1(d) shows a core element of gyro for absolute rotation sensing of the frequency splitting ROG.[6,39] Brillouin optical gyros,[3,4] PT-symmetric optical gyros,[5,6] self-injection locking gyros,[40] etc., could lead to the frequency splitting due to the Sagnac effect. A weak frequency difference produced in the frequency splitting system could result in an intensity difference of transmission beams from counterpropagating directions.[2,11] Photonic crystal in the propagation medium is indeed be used to enhance the sensitivity of detecting the relative and absolute rotation. The working principles of them are discussed below.

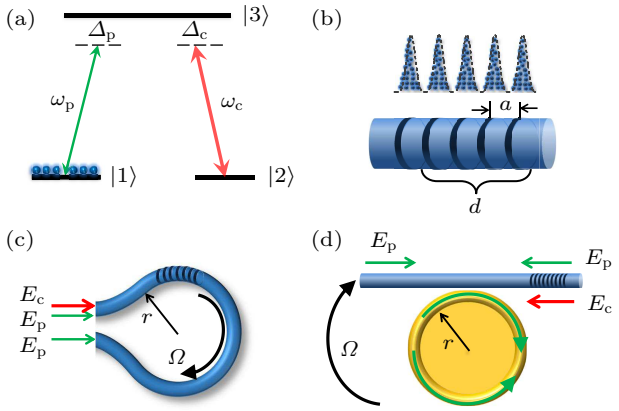


Fig. 1. (a) Energy level diagram form of a three-level Λ-type atomic system interacting with probe field $\omega_{\rm p}$ and coupling field $\omega_{\rm c}$. (b) The atoms are trapped periodically with Gaussian distribution in the photonic crystal of period and length $a = \lambda_{31}/2$ and $d = na$. (c) The core element for relative rotation sensing using Doppler effect with stationary source and frame, rotating medium. (d) Whispering gallery mode resonator (WGMR) setup for absolute rotation sensing using frequency splitting effect with corotating source and frame, stationary medium. The core rotation-sensing element can be composed of micro-resonators such as WGMR, waveguide-type ring resonator (WRR), and micro-fiber resonator. The radius of the micro-resonator is r.

In this photonic crystal structure, the probe field may experience PBG with transmission peak, which can be verified by utilizing the transfer-matrix method.[24] In brief, the first step is to construct a transfer matrix M_j of the j-th single period, which should be decomposed into, e.g., 100 sublayers of the same thickness δ_x ($\ll a$) but of different atomic densities $N(x_l)$ with ($l \in 1, 100$). The transfer matrix $m_j(x_l)$ of each sublayer is the product of a propagation matrix with a discontinuity matrix, whose coefficients are given by the Fresnel coefficients,[41] and is related to the elementary reflection and transmission coefficients, r_j and t_j, as follows:

$$m_j(z_l) = \frac{1}{t_j(z_l)}\begin{bmatrix} t_j^2(x_l) - r_j^2(z_l) & r_j(z_l) \\ -r_j(z_l) & l \end{bmatrix}. \tag{4}$$

Then $M_j = m_j(z_1)\cdots m_j(z_l)\cdots m_j(z_{100})$. The second step is to attain the transfer matrix for the whole atomic sample of length

$d = na$. Then it is easy to calculate the probe transmissivity

$$T_n(\omega_p') = |1/M_{22}|^2, \tag{5}$$

with $M_{(i,j)}$ being one matrix element of the total transfer matrix M.

In the rest frame, the frequency-dependent transmissivities $\mathcal{T}(\omega)$. from CW and CCW directions are reciprocal. However, in the lab frame (the core sensing element is set to rotate with an angular velocity Ω), at a given incident frequency ω', the transmissivities $\mathcal{T}(\omega')$ are different between the CW and CCW directions due to the frequency difference. Doppler effect can give rise to two different rest frame frequencies, or the frequency splitting system can lead to the frequency difference from the Sagnac effect. Generally, for Gaussian pulse of central frequency ω_p' and pulse bandwidth $\Delta\omega = c/\mathcal{L}'$ (c is the velocity of light in a vacuum, $\mathcal{L}'$ is the spatial length of pulse) propagating through the rotating multilayer along CW and CCW directions, the corresponding lab frame transmissivity need to be written as[38]

$$T_\pm(\omega_p') \simeq \frac{\mathcal{L}'}{c\sqrt{2\pi}} \int_{-\infty}^{\infty} \mathrm{d}\omega' \, \mathrm{e}^{-[(\omega'-\omega_p')^2/2\Delta\omega^2]} \times \mathcal{T}(\omega' \mp \Delta\omega_f). \tag{6}$$

As expected from the Doppler effect or frequency splitting from the Sagnac effect, the transmission peaks experienced by the CW and CCW monochromatic probe light of frequency ω' is shifted by $\Delta\omega_f$. Here, the multilayer structure we considered has a smooth frequency dependence of the transmissivity over the pulse bandwidth $\Delta\omega$. Thus, CW-CCW asymmetry in pulse transmission can be characterized by the nonreciprocity parameter $\Delta T(\omega_p') \equiv T_+(\omega_p') - T_-(\omega_p')$

From the Doppler effect, transmission peaks experienced by the CW and CCW monochromatic light of frequency ω' are shifted by $\mp\omega' \cdot \Omega r/c$, then the frequency difference between them is

$$\Delta\omega_{dop} = \left(1 - \sqrt{\frac{1-\Omega r/c}{1+\Omega r/c}}\right) \cdot \frac{c}{\lambda} \approx \frac{r}{2\lambda}\Omega, \tag{7}$$

where λ is the wavelength in the core rotation-sensing element. According to the principle of the Sagnac effect, the relationship between angular rate Ω and frequency shift $\Delta\omega_{sag}$ of ring resonator can be written as

$$\Delta\omega_{sag} = \frac{2r}{n_s\lambda}\Omega, \tag{8}$$

where n_s is the refractive index of the resonator. The frequency difference $\Delta\omega_{dop}$ and $\Delta\omega_{sag}$ can be used to sense the relative and absolute rotation rate, respectively. The detection of frequency difference is crucial for the sensitivity of gyro, and the sensitivity of gyro can be greatly improved by a sharp transmission peak.

3. Results and discussion

In this section, we explore, via full numerical calculations, how to generate and manipulate the nonreciprocal transmission in a coherently driven photonic crystal in terms of the sharp transmission peak. We first examine the probe transmissivity profiles in the rest frame ($\Omega = 0$) where the CW and CCW propagating transmission T_+ and T_- are reciprocal, as shown in Fig. 2(a). The sharp edges of the transmission peak, which are contributed by the coupling field, are useful to obtain the large nonreciprocal effects for a probe pulse with a full linewidth of $\Delta\omega = 1.0$ MHz. Meanwhile, we show the CW-CCW nonreciprocity in Fig. 2(b), where two resonance transmission peaks T_+ and T_- are split with a frequency difference.

In order to show the advantages of our scheme in frequency difference detection, we compare the results with the traditional RMOG. For traditional RMOG, transmissivity without considering the transmission loss of optical fiber can be written as[42]

$$T_{tra\pm} = (R')^2 \left[1 + \frac{2Q[\cos(\omega \pm \Delta\omega_f)\tau - Q]}{1+Q^2-2Q\cos(\omega\pm\Delta\omega_f)\tau} + \frac{(Q')^2}{1-(Q')^2} \cdot \frac{1-Q^2}{1+Q^2-2Q\cos(\omega\pm\Delta\omega_f)\tau}\right], \tag{9}$$

where the delay time $\tau = 2\pi r n_s/c$; $Q' = C(1-\alpha_C)$, $R' = (1-C^2)(1-\alpha_C)$, C and α_C are the coupling coefficient and the attenuation coefficient of resonator; $Q = Q'\,\mathrm{e}^{-\Delta\omega}$, $R = R'\,\mathrm{e}^{-\Delta\omega}$, $\Delta\omega$ is the linewidth of free-running laser. We show the traditional resonance curve (dashed line) with the same cavity size and laser linewidth, where the transmission peak of the photonic crystal is far sharper than the resonance curve in Fig. 2(a).

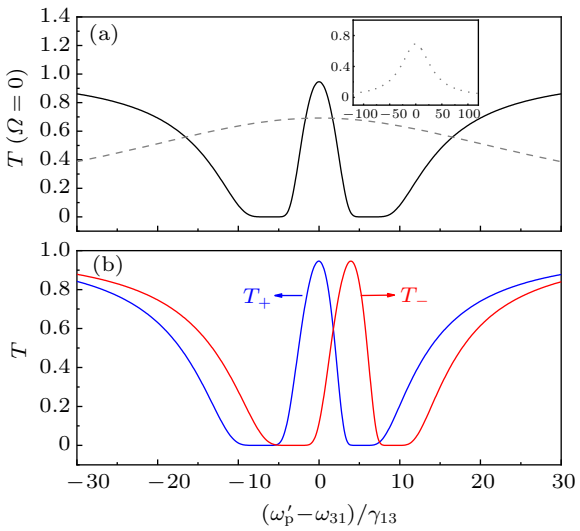


Fig. 2. (a) Rest frame transmissivity and (b) laboratory frame transmissivities under $\omega_f = 0.3\gamma$ for a photonic crystal. Other parameters are $\mathcal{L}' = 300$ m, $\gamma_{31} = \gamma_{32} = \gamma = 6$ MHz, $\gamma_{12} = 0.008\gamma$, $\Omega_c = 2\gamma$, $\Delta_c = 0$, $N_{ave} = 3.0\times10^{10}$ cm^{-3}, $\mu_{13} = 1.0\times10^{-29}$ C·m, $\lambda = \lambda_{31} = 794.969$ nm and $d = 3.0$ mm.

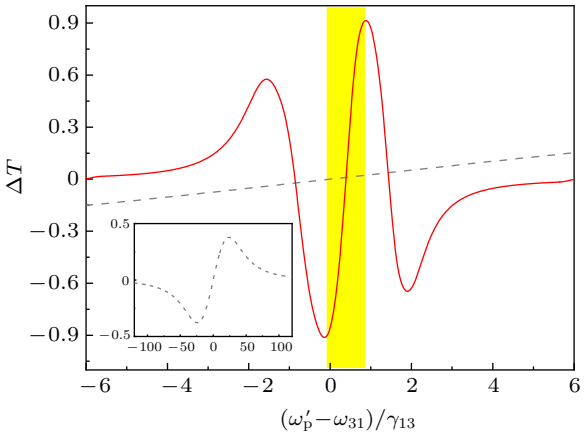


Fig. 3. Transmission nonreciprocity parameter ΔT (red soild line) with $\omega_{\rm m} = 2$ MHz and demodulation curve of traditional RMOG $\Delta T_{\rm tra}$ (gray dashed line and inset) with $\omega_{\rm mtra} = 150$ MHz as functions of the detuning of the probe central frequency $\omega_{\rm p}'/\gamma_{13}$ from the atomic resonance ω_{31}. $C = 0.95$, $\alpha_C = 0.01$, $r = 1$ cm and other parameters are the same as in Fig. 2.

In Fig. 3, we show the CW-CCW nonreciprocity parameter $\Delta T(\omega_{\rm p}') \equiv T_+(\omega_{\rm p}') - T_-(\omega_{\rm p}')$ (red solid line) and the demodulation curve of traditional ROG $\Delta T_{\rm tra} \equiv T_{\rm tra+} - T_{\rm tra-}$ with the same modulation frequency $\omega_{\rm m}$, cavity size, and laser linewidth (gray dashed line). As we can see, a sharp slope, described as $\eta = {\rm d}[\Delta T(\omega_{\rm p}')]/{\rm d}\omega_{\rm p}'$, appears within the EIT window region, which corresponds to the sharp edge of the transmission peak. The transmission nonreciprocity peak $|\Delta T|$ may reach around 90% at modulation frequency $\omega_{\rm m} = 2$ MHz. Far from the turning point, the slope of the curve $\eta = 3.3$ MHz^{-1} can be regarded as linear with the normalized and dimensionless ΔT. When gyro rotates at Ω, the frequency difference caused by the Sagnac effect $\Delta\omega_{\rm sag}$ or the Doppler effect $\Delta\omega_{\rm dop}$ will lead to the change of output light intensity $|\Delta T|$, which can be used to obtain the angular velocity rotation information.[42] Besides, the slope of the normalized transmission coefficient $\eta = 0.026$ MHz^{-1} (gray dashed line), which is two orders smaller than that of the photonic crystal structure in Fig. 1. Modulation frequency $\omega_{\rm m}$ moves the detection area to the linear area to enhance the detecting sensitivity. In addition, the direction of rotation can be easily distinguished by comparing the shifting frequency with the modulation frequency.

For the detection of relative rotation, although the frequency difference produced by the Doppler effect is slightly smaller than that produced by the Sagnac effect, the sensitivity resulted from the construction in Fig. 1(c) is about 50 times better than that of traditional resonator gyro. The frequency difference produced by the frequency splitting effect is equal to the traditional one. Thus, for the detection of absolute rotation, the sensitivity resulted from the construction in Fig. 1(d) is more than two orders better than that of traditional resonator gyro. Detecting the range of gyroscope depends on the linear region of the transmission nonreciprocity parameter ΔT highlighted in Fig. 3. As we can see, the frequency range is about 0.1γ. Then the detecting range is about ± 2600 °/s for $r = 1$ cm, which is sufficient for the gyros.

The CW-CCW nonreciprocity from a photonic crystal mentioned above can be generated by the Doppler effect for relative rotation sensing or by the frequency splitting effect for absolute rotation sensing. The underlying physical reason for the changes in optical response is that the probe susceptibility will experience a frequency shift along the direction of rotation. The probe transmissivity and absorption coefficient of the rotating atomic ensemble will be changed due to the Doppler frequency shift or splitting frequency shift experienced by the probe susceptibility. Then, if the CW-incident probe frequency is within the EIT window, the CCW-incident frequency may locate at the absorption region, which will give rise to CW-CCW nonreciprocity in probe transmission and absorption.

It is worth noting that the existence of transmission peak and rotation-induced nonreciprocity are not unique to this photonic crystal setup. Similar nonreciprocal effects can also be achieved, for example, by using the traditional rotating PBG medium. But the nonreciprocal output is low, since the transmission peak is not sharp enough.[24] In our scheme, the slope η can be enhanced by using laser-induced quantum interference because the deeply narrow EIT window can be generated by using laser-induced quantum interference. This will further give rise to transmission peak sharp enough, which is the key to high nonreciprocal output.

In Fig. 4, we further show the dependence of the slope η on the detecting sensitivity of gyro, namely, on the length of photonic crystal d, atomic density $\omega_{\rm m}$, modulation frequency $\omega_{\rm m}$, and the linewidth of free-running laser $\Delta\omega$. In Fig. 4(a), η increases with the increase of d when $d < 2$ mm, decreases with the decrease of d when $d < 2$ mm, and reaches a maximum value when d is about 2 mm; In Fig. 4(b), η increases with the increase of N_0 when $N_0 < 3.5 \times 10^1$ cm^3, decreases with the decrease of N_0 when $N_0 > 3.5 \times 10^1$ cm^{-3}, and reaches a maximum value when N_0 is around 3.5×10^1 cm^{-3}. In Fig. 4(c), η increases with the increase of $\omega_{\rm m}$ when $\omega_{\rm m} <$ 3.4 MHz, decreases with the decrease of $\omega_{\rm m}$ when $\omega_{\rm m} >$ 3.4 MHz, and reaches a maximum value when $\omega_{\rm m}$ is around 3.4 MHz. Figure 4(d) shows that η will be enhanced monotonically with decreasing the pulse linewidth $\Delta\omega$. Specifically, it increases quickly when $\mathcal{L}' < 300$ m ($\Delta\omega > 1$ MHz), changes slowly when $\mathcal{L}' > 300$ m ($\Delta\omega < 1$ MHz), and remains invariant when $\mathcal{L}' > 400$ m ($\Delta\omega < 0.75$ MHz). Thus, the detection sensitivity of η can be manipulated by modulating the length of photonic crystal d, atomic density N_0, modulation frequency $\omega_{\rm m}$, and the linewidth of free-running laser $\Delta\omega$ properly. The linear range highlighted in Fig. 3 will also be changed when these parameters are changed. Then we need to consider both the sensitivity and measurement range when modulating the parameters.

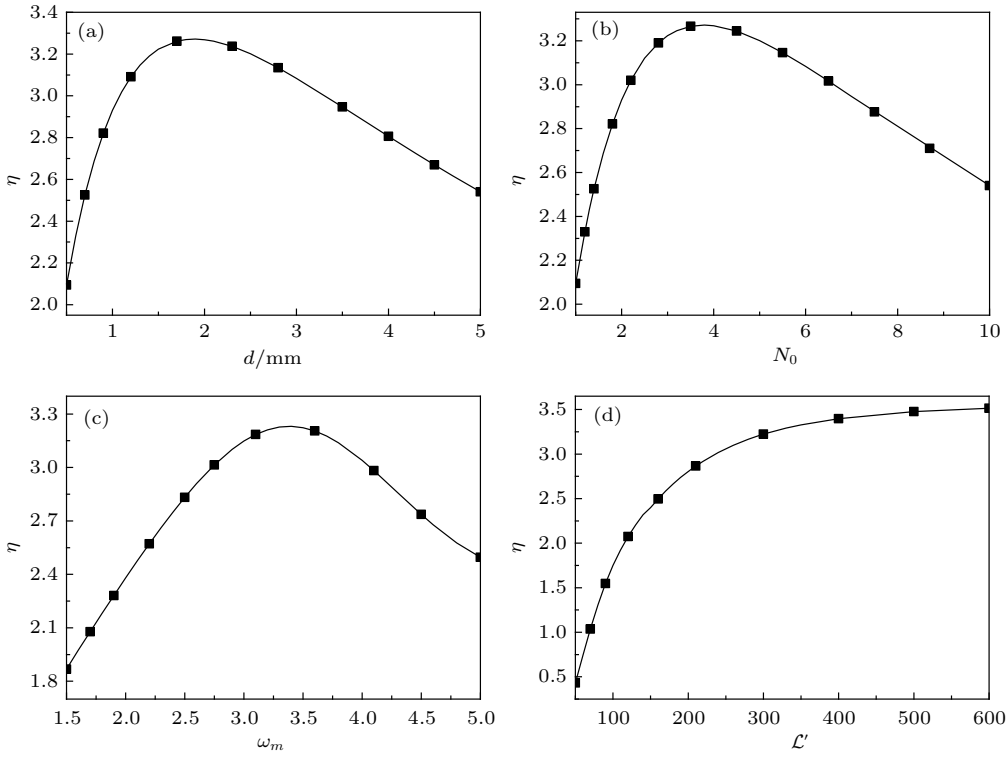


Fig. 4. The slope η of $\Delta T(\omega_p')$ as functions of (a) the length of photonic crystal d, (b) atomic density N_0, (c) modulation frequency ω_m and (d) pulse length $\mathcal{L}'$. Other parameters are the same as in Fig. 2.

At last, any level configuration leading to EIT windows can, in principle, give rise to a sharp transmission peak in a photonic crystal, which further allows for the emergence of similar nonreciprocity due to the Doppler effect or frequency splitting. However, the nonreciprocal effect depends on whether the EIT window is narrow enough and whether the transmission peak is sharp enough. The Λ configuration we considered here is the simplest and most available one to obtain the EIT window, which can lead to transmission peak sharp enough under proper parameter conditions. Thus, it can be used to achieve the ideal nonreciprocity. The nonreciprocity experienced by the probe field will arise within the frequency regions where the PBGs and transmission peak exist, namely where the two-photon resonant conditions between the probe and coupling fields are satisfied.

In an experiment, the optically controllable photonic crystal based on an EIT medium can be driven by a standing wave control laser field.[36,43] Schilke *et al.* experimentally investigated the Bragg reflection, reported the measurements of transmission and reflection spectra and their dependence on the experimental parameters.[43] According to these reported works, the scalable product of the atomic density and the sample length in our scheme can be easily realized in the experiment. What's more, in Ref. [44] the atoms could be accelerated from 0 to 10 m/s (0 to 1000 rad/s for radius $r = 1$ cm) in 100 μs with a constant transportation efficiency of more than 95%. Also, many related nonreciprocal experimental works have been reported with moving and spinning the core sensing element.[33,38] The scheme proposed in this paper is feasible in the experiment.

4. Conclusion and perspectives

In summary, the sensitivity of micro-optical gyro is enhanced utilizing the photonic crystal generated from a periodic distribution of ^{87}Rb atoms. The sharp transmission peak of electromagnetically induced transparency in a photonic crystal is sensitive to the rotation, leading to opposite frequency shifts in clockwise and counterclockwise transmission spectrums, which gives a boost to the sensitivity of the gyro system. We find that the sensitivity of gyro could be easily controlled by modulating the atomic density, modulation frequency, probe pulse width, and photonic crystal length. In this paper, we only show the working principle of the core sensitive element but do not show the design details of the gyroscope configuration, such as laser frequency locking and signal detection. We hope that high-sensitivity, miniaturized gyros can be produced based on the excellent advantages of the core sensitive element shown here with a little engineering.

References

[1] Lai Y H, Suh M G, Lu Y K, Shen B Q, Yang Q F, Wang H M, Li J, Lee S H, Yang K Y and Vahala K 2020 *Nat. Photon.* **4** 1
[2] Ma H L, Zhang J, Wang L, Lu Y, Ying D and Jin Z H 2015 *Opt. Lett.* **40** 5862
[3] Li J, Suh M G and Vahala K 2015 *Optica* **4** 346
[4] Lai Y H, Lu Y K, Suh M G, Yuan Z Q and Vahala K 2019 *Nature* **576** 65

[5] Kondratiev N M, Lobanov V E, Cherenkov A V, Voloshin A S, Pavlov N G, Koptyaev S and Gorodetsky M L 2017 *Opt. Express* **25** 28167
[6] Ren J, Hodaei H, Harari G, Hassan A U, Chow W, Soltani M, Christodoulides D and Khajavikhan M 2017 *Opt. Lett.* **42** 1556
[7] Hokmabadi M P, Schumer Alexander, Christodoulides D N and Khajavikhan M 2019 *Nature* **576** 70
[8] Biberman A, Shaw M J, Timurdogan E, Wright J B and Wattset M R 2012 *Opt. Lett.* **37** 4236
[9] Khial P P, White A D and Hajimiri A 2018 *Nat. Photon.* **12** 671
[10] Ma H L, Zhang J J, Wang L L and Jin Z H 2015 *Opt. Express* **23** 15088
[11] Wang J J, Feng L S, Tang Y C and Zhi Y Z 2015 *Opt. Lett.* **40** 155
[12] Wang J J, Ma H L, Li H Z and Jin Z H 2017 *Opt. Lett.* **42** 3658
[13] Matsko A B, Liang W, Savchenkov A A, Ilchenko V S and Maleki L 2017 *Phys. Lett. A* **382** 2289
[14] Shahriar M S, Pati G S, Tripathi R, Gopal V, Messall M and Salit K 2007 *Phys. Rev. A* **75** 053807
[15] Zhang E K, Yang L, Xue B, Gao Z X and Zhang Y G 2018 *Opt. Eng.* **57** 085106
[16] Xie C F, Tang J, Cui D F, Wu D J, Zhang C F, Li C M, Zhen Y Q, Xue C Y and Liu J 2016 *Opt. Lett.* **41** 4783
[17] Liang W, Ilchenko V S, Savchenkov A A, Dale E, Eliyahu D, Matsko A B and Maleki L 2017 *Optica* **4** 114
[18] Li H Z, Lin Y, Liu L, Ma H L and Jin Z H 2020 *Opt. Express* **28** 18103
[19] Wang J J, Feng L S, Wang Q W, Jiao H C and Wang X 2016 *Opt. Lett.* **41** 1586
[20] Harris S E 1997 *Phys. Today* **50** 36
[21] Lukin M D, Fleischhauer M, Scully M O and Velichansky V L 1998 *Opt. Lett.* **23** 295
[22] Li J H, Qu Y, Yu R and Wu Y 2018 *Phys. Rev. A* **97** 023826
[23] Zhang Y, Liu Y M, Tian X D, Zheng T Y and Wu J H 2015 *Phys. Rev. A* **91** 013826
[24] Artoni M, La Rocca G C and Bassani F 2005 *Phys. Rev. E* **72** 046604
[25] Petrosyan D 2007 *Phys. Rev. A* **76** 053823
[26] Hua S Y, Wen J M, Jiang X S, Hua Q, Jiang L and Xiao M 2016 *Nat. Commun.* **7** 13657
[27] He B, Yang L, Jiang X S and Xiao M 2018 *Phys. Rev. Lett.* **120** 203904
[28] Zhang H L, Huang R, Zhang S D, Li Y, Qiu C W, Nori F and Jing H 2020 *Nano Lett.* **20** 7594
[29] Kang M S, Butsch A and Russell P St J 2011 *Nat. Photon.* **5** 549
[30] Zaman T R, Guo X and Ram R J 2007 *Appl. Phys. Lett.* **90** 023514
[31] Maayani S, Dahan R, Kligerman Y, Moses E, Hassan A U, Jing H, Nori F, Christodoulides D N and Carmon T 2018 *Nature* **558** 569
[32] Jing H, Lü H, Özdemir S K, Carmon T and Nori F 2018 *Optica* **5** 1424
[33] Lü H, Jiang Y J, Wang Y Z and Jing H 2017 *Photonics Res.* **5** 367
[34] Jiang Y, Maayani S, Carmon T, Nori F and Jing H 2018 *Phys. Rev. Appl.* **10** 064037
[35] Serebryannikov A E 2009 *Phys. Rev. B* **80** 155117
[36] Wang D W, Zhou H T, Guo M J, Zhang J X, Evers J and Zhu S Y 2013 *Phys. Rev. Lett.* **110** 093901
[37] Yang L, Zhang Y, Yan X B, Sheng Y, Cui C L and Wu J H 2015 *Phys. Rev. A* **92** 053859
[38] Horsley S A R, Wu J H, Artoni M and La Rocca G C 2013 *Phys. Rev. Lett.* **110** 223602
[39] Liang W, Savchenkov A, Ilchenko V, Griffith R, Cuir E D, Kim S, Matsko A and Maleki L 2017 *Opt. Lett.* **42** 4736
[40] Geng J T, Yang L, Zhao S H and Zhang Y G 2020 *Opt. Express* **28** 32907
[41] Bendickson J M, Dowling J P and Scalora M 1996 *Phys. Rev. E* **53** 4107
[42] Fei Y, He Y M, Wang X D, Yang F H and Li Z F 2018 *Chin. Phys. B* **27** 084213
[43] Schilke A, Zimmermann C, Courteille P W and Guerin W 2011 *Phys. Rev. Lett.* **106** 223903
[44] Kuhr S, Alt W, Schrader D, Müller M, Gomer V and Meschede D 2001 *Science* **293** 278